Mapping Variations in Crop Growth and Irrigation in a Crop Field with Landsat-Derived Spectral Products

Niharika Sharma[1], Katie D. Magana[2], Sajith Variyar V. V.[1], Ramesh Sivanpillai[2]

[1]Amrita School of Artificial Intelligence, Coimbatore, Amrita Vishwa Vidyapeetham, India.
(kushi711557@gmail.com, ORCID: 0009-0009-6987-7293; vv.sajithvariyar@cb.amrita.edu, ORCID: 0000-0003-3944-8155)

[2]Wyoming GIS Center, School of Computing, University of Wyoming, Laramie, WY 82071, USA.
(sivan@uwyo.edu, ORCID: 0000-0003-3547-9464)

Keywords: Sprinkler Irrigation, Mean Shift Clustering, NDVI, NDMI, Unsupervised Machine Learning.

Abstract

The shift from conventional irrigation methods to sprinkler systems is intended to improve accuracy and efficiency; however, it requires thorough validation of the uniformity of water distribution. This research focuses on a particular agricultural issue related to possible coverage deficiencies in a 33-hectare field that has recently been fitted with a sprinkler system. The main goal was to detect spatial discrepancies in crop growth utilizing Landsat-derived data from the 2024-25 growing season. The analytical approach employed was Mean Shift Clustering (MSC), a non-parametric, unsupervised machine learning technique, to segment images of the Normalized Difference Vegetation Index (NDVI). In contrast to parametric techniques that necessitate predetermined cluster counts, MSC interprets the flattened 1D NDVI feature space as an empirical probability density function. By applying an adaptive bandwidth (calculated using a 0.1 quantile estimate), the algorithm iteratively adjusted data points towards high-density modes to autonomously ascertain the optimal number of growth zones. Concurrently with this machine learning-driven segmentation, a visual examination of Normalized Difference Moisture Index (NDMI) pixels was conducted to evaluate moisture levels. The MSC algorithm identified six distinct spectral clusters with the following average NDVI values: Cluster 0 (0.84), Cluster 1 (0.72), Cluster 2 (0.82), Cluster 3 (0.71), Cluster 4 (0.19), and Cluster 5 (0.68). Importantly, both the unsupervised NDVI clustering and the NDMI moisture assessment produced consistent findings: no significant spatial anomalies or indications of water stress were observed. The study verified that the sprinkler system delivered a uniform water supply, effectively addressing the farmer's concerns regarding variations in irrigation.

1. Introduction

Agriculture is responsible for nearly 70% of the global freshwater withdrawals (Xie et al., 2021). In a time characterized by increasing water scarcity and food demand driven by population growth, the agricultural industry confronts a significant optimization challenge: enhancing yield while reducing resource usage. Conventional flood irrigation, although widespread, often leads to considerable water loss and uneven distribution across fields (Moursy et al., 2023). In contrast, sprinkler irrigation, provide improved efficiency but necessitate a considerable financial investment. For farmers who implement these expensive systems, the return on investment is largely contingent upon performance assessment; it is crucial to evaluate whether the infrastructure achieves the expected consistency in water distribution and subsequent crop development. As a result, remote sensing has emerged as a vital instrument for validation, facilitating the identification of spatial inconsistencies and allowing for targeted strategies to address issues where mechanical or environmental factors hinder irrigation effectiveness.

To promote the sustainable management of water resources, the assessment of irrigation system performance has evolved from basic volumetric measurements to sophisticated, multidimensional analyses employing satellite remote sensing technologies (Bwambale et al., 2022). The Landsat program, acquiring multispectral imagery at 30 m spatial resolution since Landsat 5, has emerged as the benchmark for monitoring at the field scale. However, the utility of this resolution is intrinsically linked to field geometry; for a field to be accurately monitored, it must be large enough to show up in Landsat image pixels. In many regions, particularly where smallholder farming or complex land-fragmentation prevails, fields may be too small to be resolved individually, as their spectral signatures become mixed with surrounding non-crop features within the 30 m $\times$ 30 m pixel grid. Recent advancements, exemplified by the creation of the LANID (Landsat-based Irrigation Dataset), have demonstrated that Landsat spectral products can accurately delineate irrigation frequency and extent with an accuracy exceeding 90% across a variety of cropping systems (Xie et al., 2021). This methodological progression enables researchers to shift focus from coarse regional approximations to precise delineations of field-specific management zones.

While the mapping of irrigation extent is well-established, assessing irrigation effectiveness within individual fields necessitates monitoring crop responses. There are various studies, that are done for understanding the effectiveness of different types of irrigation across different crops. Apart from this, there are studies, which utilize satellite images and vegetation indices derived from multispectral data. The NDVI, derived from Landsat imagery, serves as the principal indicator for this purpose. (Zea et al., 2025), revealed a significant correlation between Landsat-derived NDVI values and agricultural energy inputs, thereby validating NDVI as a reliable proxy for crop vigor and irrigation responsiveness. (Saadi et al., 2015), successfully integrated Landsat time-series data with the FAO-56 water balance model to estimate Net Irrigation Depth by tracking spectral changes in crops throughout the growing season.

The exclusive dependence on the NDVI presents certain lim-

itations. A comprehensive review of crop identification methodologies highlights that NDVI experiences saturation in dense vegetation canopies, specifically when the Leaf Area Index exceeds 3, thereby complicating the differentiation between adequately and excessively irrigated areas (Niţu et al., 2025). (Gu et al., 2008), stated that as the canopy closes, the red light absorption reaches a peak, causing the NDVI values to plateau even as biomass continues to increase. This lack of sensitivity in high-leaf-density environments often necessitates the use of narrow-band indices or modified vegetation indices to accurately capture variations in crop vigor (Mutanga and Skidmore, 2004). In contrast to the NDVI, which measures a different biophysical condition, the NDMI, which is derived from the near-infrared and short-wave infrared bands of Landsat imagery, is better suited for identifying water stress because it targets vegetation water content. A recent 2024 investigation focusing on maize crops revealed that seasonal variations in NDMI exhibit a strong negative correlation ($R^2 = 0.62$) with soil moisture deficits, thereby serving as a reliable proxy for water availability even in instances where NDVI values remain constant (Lykhovyd and Sharii, 2024). It is important to note that while the Landsat satellite has a revisit cycle of 16 days, the ultimate goal of the Landsat mission is to maintain two operational satellites in orbit at the same time. By interweaving the orbital paths of the two satellites, the revisit cycle is shortened to 8 days. However, data gaps may still be created by the presence of cloud cover, sometimes requiring the combination of Landsat data with other data sources (Wang et al., 2021).

The conversion of spectral maps into practical irrigation zones necessitates the application of unsupervised machine learning techniques. Among these, K-Means clustering is extensively employed to partition agricultural fields into homogeneous yield zones. For instance, a study conducted in 2025 on crop suitability utilized K-Means clustering to classify Landsat pixels according to soil and spectral characteristics, with cluster validation performed using the Elbow Method (Jamshed et al., 2025). Although K-Means has demonstrated effectiveness in such contexts, the algorithm inherently assumes spherical cluster shapes and requires the predetermined specification of the number of clusters (k). This constraint can lead to the imposition of artificial geometric boundaries on naturally occurring, irregular spatial variations within complex field environments.

This constraint warrants the utilization of density-based techniques such as MSC. Studies in the domain of agricultural segmentation indicate that MSC is especially advantageous for high-resolution imagery, as it obviates the need for specifying the number of clusters a priori (Friedman et al., 2013). Rather than relying on predetermined cluster counts, MSC identifies the modes within the spectral distribution, thereby enabling the detection of stress regions with complex, nonlinear shapes—such as curved arid patches influenced by topography or soil characteristics—that conventional methods like K-Means tend to artificially partition. By dynamically adjusting to the local density within the Landsat spectral feature space, MSC facilitates a more empirically grounded delineation of moisture content (Friedman et al., 2013).

Building on this foundation, the main aim of this research was to outline spatial differences in crop growth and to validate the uniformity of irrigation using Landsat-derived spectral products. The primary method employed was MSC applied to the NDVI feature space, a technique chosen for its capacity to organize pixels based on spectral density without requiring prior assumptions about the number of clusters.

Simultaneously, a visual analysis of the NDMI was performed to offer a direct evaluation of pixel-level moisture content, acting as a safeguard against possible NDVI saturation. By merging the algorithmic segmentation of MSC with the moisture-sensitive attributes of NDMI, this research sought not only to verify whether the sprinkler system produced uniform growth but also to reveal hidden spatial variations that traditional methods might overlook. Ultimately, these findings equip the farmer with actionable, data-driven insights to enhance irrigation planning and promote sustainable resource management.

2. Methodology

2.1 Study Area and Preprocessing

The study was conducted on a 33-hectare agricultural field located in Holtville, California, within the Lower Colorado River Basin—a region of significant importance to U.S. agriculture that also faces substantial challenges related to water resource management. Irrigation water in this area is provided by the Imperial Irrigation District, one of the oldest and largest irrigation districts in the United States. The focus of this research was to monitor the effect of switching to a sprinkler irrigation system. This setting presented a valuable opportunity to evaluate the efficiency of sprinkler irrigation in water distribution relative to traditional flood irrigation techniques.

Red cabbage was planted in the field during the growing season of 2024-25, which served as a continuous subject for longitudinal study. Although the field practiced staggered planting, further insight into this practice was gained through spatial analysis, where the Mean Shift algorithm divided the field into six to seven zones based on spectral characteristics. This division of the field by the algorithm reflected the practical conditions of the field, where the dates of planting were not homogeneous. For example, based on the clusters derived from the model, it was observed that the zone in the western part of the field had attained maturity and was being harvested, while the eastern zone was simultaneously being planted. The field's moderate size, well-defined boundaries, and recent conversion to sprinkler irrigation made it particularly suitable for detailed satellite-based monitoring and analysis. To assess crop development, Landsat satellite imagery was employed as the primary data source. The Landsat program, managed by the U.S. Geological Survey, provides freely accessible multispectral images along with various pre-processed spectral indices.

This investigation primarily utilized the NDVI, a widely recognized metric for assessing plant health. NDVI measures vegetation greenness and vigor, rendering it especially effective for tracking crop growth and detecting spatial variability within the field. Multi-temporal Landsat images covering both early and late stages of the 2024–25 growing season were analyzed to capture temporal changes in vegetation and to assess the overall uniformity of the sprinkler-irrigated field.

A total of seven NDVI images, shown in Table 1 with their acquisition dates, were acquired for the study area between December 2024 and February 2025. A sample image from the acquired images is shown in Fig 1. NDVI values were divided the pixel values by 10,000 to convert them into the standard NDVI range between -1 and +1. Pixels with missing or invalid

data (NaNs) were excluded from subsequent analyses. The initial image in the series was designated as the spatial reference, and all subsequent images were resampled to conform to this reference geometry, ensuring consistent spatial alignment for comparative evaluation.

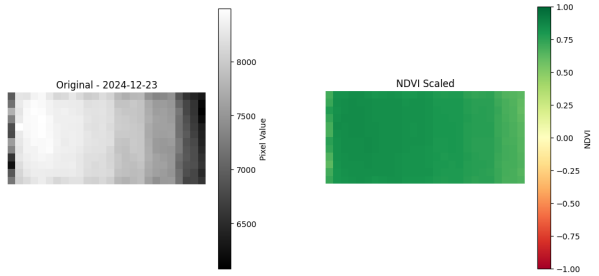

(a) (b)

Figure 1. Data Preprocessing Visualization (December 23, 2024): Figure 1a (Grayscale) shows the raw Landsat image based on the original digital values, as shown by the scale in the legend. The grayscale image clearly shows a strong banding effect, ranging from light to dark gray. These differences are not noise but rather an indication of the staggered planting schedules in the field's different operational areas. Figure 1b (Color) shows the image processed by dividing the raw values by 10,000 to calculate the standard NDVI. In this image, the right-hand legend indicates the normalized range from -1 to +1, where red to orange indicates bare ground or areas planted later in the season and dark green indicates mature vegetation. This image further supports the conclusion that the bands in the raw image correspond to the seasonal growth of the crop, as the algorithm is able to distinguish between the high-NDVI mature areas and the lower-NDVI areas planted later in the season.

In addition to the NDVI-based growth assessment, this study included the NDMI as a supplementary metric. While NDVI focuses on assessing vegetation vigor, NDMI utilizes the Near-Infrared (NIR) and Short-Wave Infrared (SWIR) bands to estimate the water content present within the canopy. The primary aim was to segment these moisture maps to identify any distinct hydric zones or spatial variations in water availability that may not be readily apparent in the vegetation index.

For this analysis, NDMI values were extracted for each pixel corresponding to the collected Landsat scenes. These moisture profiles were then visualized to enable a comprehensive spatial analysis. A methodical visual examination was conducted to detect potential gradients or anomalies related to moisture stress throughout the field.

2.2 Mean Shift Clustering

2.2.1 Theoretical basis To identify clusters within the agricultural field exhibiting comparable levels of vegetation vigor, the MSC algorithm was applied to imagery derived from the NDVI. As mentioned earlier in this manuscript, the MSC is able to identify the modes (local maxima) of an estimated probability density function (PDF) based on the data (Friedman et al., 2013). This is especially useful in remote sensing, as it is able to well define discrete classes that are formed due to variations in soil type, slope, and aspect, which form sharp boundaries in the field.

The MSC algorithm uses NDVI image from Landsat imagery as its input, rather than relying on pre-specified cluster numbers

Table 1. Field images with their acquisition dates.

Date of acquisition	Image
2024–12–23	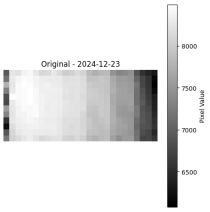
2025–01–08	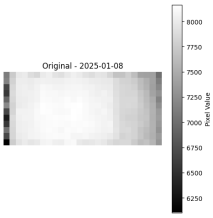
2025–01–24	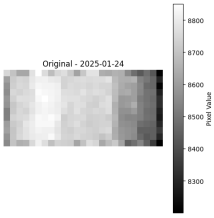
2024–02–01	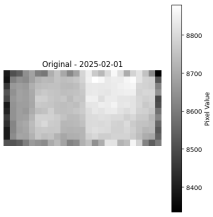
2025–02–09	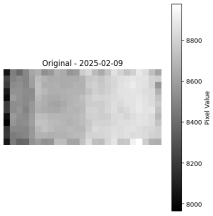
2025–02–17	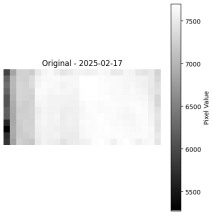
2025–02–25	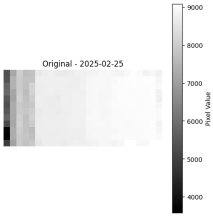

like centroid-based methods. Instead, it applied kernel density estimation to treat the feature space as a probability density function, grouping pixels into clusters based on their convergence to local density maxima. The expected output is a segmented map that represents distinct levels of vegetation vigor and irrigation uniformity.

The algorithm follows a unified mathematical and procedural execution:

1. **Initialization and Input Mapping:** Each pixel of the NDVI image is treated as an individual data point in the set of n data points as shown in Eq.1

$$\mathbf{X} = \{\mathbf{x}_1, \mathbf{x}_2, \ldots, \mathbf{x}_n\}, \quad \mathbf{x}_i \in R^d \tag{1}$$

   In this application, $\mathbf{x}_i$ represents the specific NDVI value of pixel i, and $d = 1$ for single-date analysis (or $d = 7$ for the multi-temporal stack). Hence X is the input NDVI image.

2. **Neighbourhood Definition and Density Estimation:** A search window with radius h is established around each data point. The PDF at any point $\mathbf{x}$ is estimated using a kernel density estimator as shown in Eq.2

$$\hat{f}(\mathbf{x}) = \frac{1}{nh^d} \sum_{i=1}^{n} K\Big(\frac{\mathbf{x} - \mathbf{x}_i}{h}\Big) \tag{2}$$

   The bandwidth parameter (h) regulates the window size for local density estimation, while $K(\cdot)$ is a Gaussian kernel function that weights the influence of neighboring pixels based on their spectral proximity to the center x, calculated as shown in Eq.3

$$K(\mathbf{x}) = \exp\left(-\frac{1}{2}\|\mathbf{x}\|^2\right) \tag{3}$$

3. **Mean Shift Vector Computation:**The algorithm calculates the local mean (center of mass) for all points within the search window. The Mean Shift vector, $\mathbf{m}(\mathbf{x})$, represents the gradient direction of the estimated density and points toward regions of higher data density, calculated as shown in Eq.4

$$\mathbf{m}(\mathbf{x}) = \frac{\sum_{i=1}^{n} \mathbf{x}_i \, g\left(\left\|\frac{\mathbf{x}-\mathbf{x}_i}{h}\right\|^2\right)}{\sum_{i=1}^{n} g\left(\left\|\frac{\mathbf{x}-\mathbf{x}_i}{h}\right\|^2\right)} - \mathbf{x} \tag{4}$$

   where $g(\cdot) = -K'(\cdot)$ is the derivative of the kernel function.

4. **Iterative Update and Convergence:** The center of the search window is shifted toward the newly computed local mean using the iterative update rule, calculated as shown in Eq.5

$$\mathbf{x}_{t+1} = \mathbf{x}_t + \mathbf{m}(\mathbf{x}_t) \tag{5}$$

   Iterations are performed until the shift in the window's centre is smaller than the convergence threshold ε. In this experiment pre-defined value from library was taken but user can define it as well. At this stage, the movement is considered negligible ($\|\mathbf{m}(\mathbf{x}_t)\| < \varepsilon$), confirming that the algorithm has reached a stable peak in the NDVI probability density.

5. **Cluster Formation and Output:** Once the iteration concludes, all data points (pixels) that converge to the same density peak are grouped together, forming a cluster. The resulting output is a segmented NDVI image where regions with similar vegetation vigor and growth patterns are assigned the same label, allowing for the pinpointing of anomalies across the cropping season.

2.2.2 Experimental Setup Each NDVI image was transformed into a one-dimensional feature array $X \in R^{n\times 1}$, while preserving pixel coordinates to enable spatial reconstruction following clustering. The computational workflow was implemented in Python within the Google Colab environment. The bandwidth parameter (h), which regulates the window size for local density estimation, was automatically determined using the *estimate_bandwidth* function from the `scikit-learn` library (Pedregosa et al., 2011) with a quantile value of 0.1. This adaptive selection ensures that the search radius is tailored to the statistical properties of each image, thereby accommodating variations arising from seasonality and illumination conditions. Subsequently, the Mean Shift Clustering (MSC) implementation from `sklearn.cluster` (Pedregosa et al., 2011) was applied within this feature space to identify clusters based on the convergence of density peaks. Each pixel was assigned a label corresponding to its nearest mode, resulting in a segmented NDVI image in which regions exhibiting similar vegetation vigor were grouped together. To capture the temporal evolution of crop vigor, NDVI images from seven Landsat acquisitions spanning the 2024–2025 cropping season were compiled into a composite multi-temporal dataset. This stacking enabled the assessment of both spatial and temporal variations in crop growth patterns. The resulting multi-temporal segmentation provided a robust basis for evaluating field-level variability and identifying areas exhibiting consistent or anomalous growth behavior.

3. Results

3.1 Spatiotemporal Evolution of Crop Vigor

It is worth noting that because of the staggered planting schedule, the eastern area was left unplanted during the first three acquisition dates, as can be seen in Fig 2a-c, providing a strong spectral contrast between this area and the rest of the field that was planted earlier. The unsupervised MSC analysis conducted on each image demonstrates a notable transition from early-season diversity to late-season consistency as shown in Fig 2.

Image 2a-c (Dec 23 – Jan 24): The imagery observed in the early season is marked by considerable heterogeneity and fragmented clusters as can be seen in Fig 2b and 2c. Throughout all acquisition dates, the predominant portion of the field is consistently assigned to Cluster 0 (brick red in color), signifying that the majority of pixels exhibit similar NDVI values and, therefore, correspond to similar stages of crop development. This pattern implies that these regions are adequately irrigated, facilitating uniform crop growth. In addition to the primary cluster, multiple smaller clusters (like green and purple) appear in a staggered, banded arrangement, indicating comparable growth conditions within distinct strips of the field. The spectral signal is largely determined by the contrast between the early-planted strips (emerging vegetation) and the later-planted strips (bare soil). The mean NDVI of the brick red cluster in Fig 2a-c is around 0.84 indicating that the western portion of the field has the crops that are in peak growth stage. Meanwhile the other

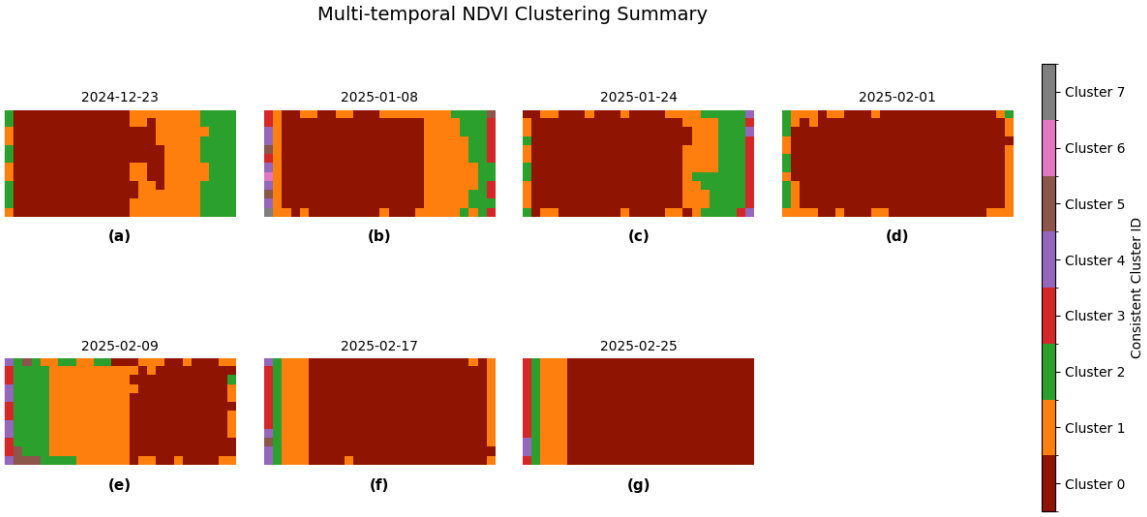

Figure 2. Temporal evolution of crop vigor (Dec 2024 – Feb 2025). The panel displays the MSC segmentation for each of the seven total acquisitions, with the specific acquisition date included in each file name. Cluster colors are assigned in decreasing order of cluster size, with larger pixel populations appearing first in the color scale. Crucially, in the final three images (e-g), the westernmost parts of the field are visible as clear clusters because they have already been harvested. Note the progression from chaotic, fragmented clusters in the early dates (a–c) to a single, uniform high-vigor zone in the later dates (e–g), demonstrating the effectiveness of the irrigation system in achieving field-wide consistency.

clusters are more scattered and exhibit lower NDVI values (orange cluster-0.76, green cluster-0.80).

Image 2d (Feb 01, 2025): This date indicates the peak of spectral convergence. The MSC algorithm reveals a single, dominant high-vigor cluster (Cluster 0, brick red in color) that covers most of the field. Mean NDVI of brick red cluster here is 0.88, indicating high growth across the entire field. At this stage, the crop canopy has closed completely across all strips. Even though the strips were planted on different dates, the later-planted strips have developed a sufficient leaf area index (LAI) to mask the underlying soil, making them spectrally indistinguishable from the earlier strips. We did not find any major variation in crop growth after switching to the sprinkler system

Image 2e (Feb 09, 2025): A re-emergence of clustering is observed. Unlike a simple linear trajectory, the single cluster from Feb 01 has fragmented into multiple distinct clusters. This phenomenon does not signify a regression in health; instead, it indicates differential maturation. The strips that were planted earliest (Cluster 1, the orange cluster, with mean NDVI of 0.85) are likely entering the reproductive/senescence phase (as indicated by a slight reduction in NDVI due to energy allocation towards fruit/head formation), while the strips planted later remain in the peak vegetative phase (exhibiting maximum NDVI). The clustering algorithm captures this subtle phenological differentiation, effectively 'rediscovering' the strip pattern that was previously concealed during the peak vegetative stage.

Image 2f–g (Feb 17 – Feb 25): The field reaches its ultimate maturity classifications. The clustering remains stable, with variations primarily limited to the edges of the field. Cluster 0 (with mean NDVI of 0.82 and brick red color has now shifted to eastern side of the field). This side is showing an increase later as a result of its later plantation date. The earlier planted strips (green cluster with mean NDVI of 0.76 and orange cluster with mean NDVI of 0.70) show lower NDVI values as a result of them reaching senescence phase. The ongoing presence of lower values on the western boundary edge throughout the series is recognized as a geometric artifact (Adjacency Effect) resulting from shadows or boundary characteristics, rather than a lack of irrigation.

3.2 Composite Spatial Zoning

To establish a clear distinction between transient phenological stages and permanent field conditions, an analysis of a temporal composite covering the entire growing season was performed. By stacking all seven images, the MSC algorithm reduced any possible fluctuations to uncover the stable management zones of the field. The results, visualized in Figure 3, indicate that the field is not a single uniform block, but rather composed of two distinct cultivation zones flanked by structural boundaries. The statistical characteristics of these zones are outlined in Table 2.

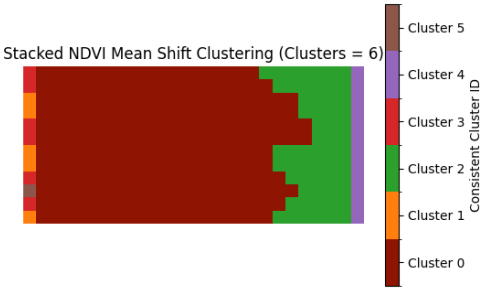

Figure 3. Composite Management Zone Map. The map reveals a spatial bipartition of the field into a Primary Core (Brick red, Cluster 0) and a Secondary/Lagging Zone (Green, Cluster 2). The true field edges are restricted to the vertical extremes: the Western Boundary (Orange/Red) and the Eastern Boundary (Purple).

1. **The Primary Production Zone** (Cluster 0): The analysis revealed that the Western and Central sectors are the predominant features (Brick red in Fig. 3), consisting of 229 pixels(about 20.61 hectares) exhibiting the highest mean NDVI (0.84). This area represents the primary productive

Table 2. Summary statistics of NDVI clusters

Cluster ID	Number of pixels	Mean NDVI	Min NDVI	Max NDVI	Interpretation
0	229	0.835093	0.790557	0.845986	Primary Core: The western/central block showing optimal, synchronized maturity.
1	5	0.724440	0.701271	0.739143	Western Interface: "Soft" edge pixels along the western fence line.
2	59	0.818788	0.786157	0.834357	Secondary Zone: The eastern block. Valid crop with a lagging cumulative signal due to later planting.
3	6	0.713098	0.686371	0.730586	Structural Shadow: Pixels likely affected by shadows or physical barriers on the west.
4	12	0.194774	0.189514	0.198386	Eastern Edge: The hard boundary marking the end of the field on the east.
5	1	0.677286	0.677286	0.677286	Artifact: Discrete point noise on the western boundary.

zone. Its high spectral uniformity indicates that, for the majority of the field, the crop has achieved optimal canopy closure and phenological synchronization, reflecting a successful response to the sprinkler irrigation.

2. **The Secondary Cultivation Zone** (Cluster 2): In contrast to the core, a unified block of 59 pixels(5.31 hectares) was detected in the Eastern sector (Green in Fig. 3). This zone represents later planting area, distinct from the edge artifacts. Its separation from the core and slightly lower mean NDVI (0.81) can be attributed to phenological offset. This section corresponds to the specific strips that were planted last according to the farmer's schedule. Although the crop in this area is healthy, its cumulative growing period was shorter than that of the Primary Zone, leading to a statistically distinct seasonal signature.

3. **Boundary Artifacts** (Clusters 1, 3, 4, 5): The remaining clusters define the physical boundaries of the field, where spectral mixing is observed between agricultural and non-arable regions of the field.

   (a) Western Boundary (Clusters 1, 3, 5): A narrow, varied vertical strip (Orange/Red/Brown) delineates the boundary with the western fence line and its infrastructure.

   (b) Eastern Boundary (Cluster 4): A singular vertical strip (Purple) indicates the clear transition between the Secondary Zone and the adjacent open land.

Meanwhile to detect possible gradients or abnormal patterns referencing moisture stress, a systematic visual investigation was conducted on the plotted NDMI values. The analysis indicated patterns resembling the patterns observed from the NDVI with respect to staggered planting sequences. To quantify these observations, NDMI values were derived from 156 sample locations for the 2024/12/23 and 2025/01/08 acquisition dates.

Here is the statistical summary of these samples.

- On 23 December 2024, the NDMI achieved an average of 0.63772 with a standard deviation of 0.0887. Lower values clustered in the east correlated to barren areas where growth had not yet started.
- On 2025/01/08, the NDMI average was 0.65778 while the standard deviation was 0.05158.

The standard deviation values are consistently low with no distinct patches of low moisture, suggesting a uniform distribution of water in the study area. As there were no anomalies seen, nor moisture-stress gradients detected, these figures suggest that the coverage of the sprinkler irrigation system was uniform. Considering the homogeneity of these statistics led to the conclusion not to use a more complex classification algorithm and the need for NDMI-based segmentation was excluded.

4. Conclusion

From the integrated findings of our analysis, we can infer that the sprinkler irrigation system successfully upheld uniform crop vigor across the entire 33-hectare study area, apart from the variation caused by differences in planting dates. With results from MSC analysis of seven NDVI values and visualization of corresponding NDMI values, we arrived at the same conclusion.

The analysis illustrated a clear timeline for crop development. Initially, the field appeared patchy and variable, reflecting the farmer's staggered strip-planting schedule. However, a distinct trend of 'catching up' emerged as the season progressed. The variation in NDVI values decreased significantly between the early and late stages. This confirms that the irrigation provided the consistent support necessary for the later-planted strips to mature and match the rest of the field, resulting in a uniform canopy by the end of the season.

Moreover, the strength of the chosen machine learning method was crucial in assessing the irrigation performance. The MSC algorithm was found to be effective in segmenting the field according to spectral signatures, enabling us to verify that the detected variations were not due to irregular water distribution or in simpler words, water was reaching all parts of the field. By precisely clustering the data, the algorithm illustrated that despite staggered planting, the irrigation levels were sufficiently consistent to uphold uniform physiological potential throughout all zones, effectively eliminating noise that could be misinterpreted as irrigation inefficiency.

The spatial clustering partitioned the field into two main sections—the Primary Zone and the Secondary Zone—rather than a single block. Our analysis verifies that this division is due to the planting timeline (phenology) rather than irrigation discrepancies. The Secondary Zone corresponds to the area planted

last; while it displayed a slightly different spectral signature, it was not 'stressed,' merely younger.

Crucially, both techniques arrived at the same conclusion. MSC illustrated the distinct growth stages, while the NDMI Analysis corroborated that moisture levels were uniform across both zones. This consensus enhances our findings: the differences observed were biological (timing of growth), not hydrological (water scarcity). Ultimately, the transition to sprinkler irrigation effectively ensured efficient water use and uniform growth across the field.

References

Bwambale, E., Naangmenyele, Z., Iradukunda, P., Agboka, K. M., Houessou-Dossou, E. A. Y., Akansake, D. A., Bisa, M. E., Hamadou, A.-A. H., Hakizayezu, J., Onofua, O. E., Chikabvumbwa, S. R., 2022. Towards precision irrigation management: A review of GIS, remote sensing and emerging technologies. *Cogent Engineering*, 9(1), 2100573. https://doi.org/10.1080/23311916.2022.2100573.

Friedman, L., Netanyahu, N., Shoshany, M., 2013. Mean shift-based clustering of remotely sensed data with agricultural and land-cover applications. *International Journal of Remote Sensing*, 34(17), 6037–6053.

Gu, Y., Hunt, E., Wardlow, B., Basara, J., Brown, J., Verdin, J., 2008. Evaluation of MODIS NDVI and NDWI for vegetation drought monitoring using Oklahoma Mesonet soil moisture data. *Geophysical Research Letters*, 35.

Jamshed, H., Waheed, U., Mansoor, Y., Hussain, A., 2025. Unsupervised Learning for Crop Suitability Clustering Based on Soil Nutrients. *Malaysian Journal of Fundamental and Applied Sciences*, 21, 2945-2957.

Lykhovyd, P. V., Sharii, V. O., 2024. Normalised difference moisture index in water stress assessment of maize crops. *Agrology*, 7(1), 21-26. https://agrologyjournal.com/index.php/agrology/article/view/138.

Moursy, M., ElFetyany, M., Meleha, A., El-Bialy, M. A., 2023. Productivity and profitability of modern irrigation methods through the application of on-farm drip irrigation on some crops in the Northern Nile Delta of Egypt. *Alexandria Engineering Journal*, 62, 349-356.

Mutanga, O., Skidmore, A. K., 2004. Narrow band vegetation indices overcome the saturation problem in biomass estimation. *International Journal of Remote Sensing*, 25(19), 3999–4014. https://doi.org/10.1080/01431160310001654923.

Nițu, A., Florea, C., Ivanovici, M., Racoviteanu, A., 2025. NDVI and Beyond: Vegetation Indices as Features for Crop Recognition and Segmentation in Hyperspectral Data. *Sensors*, 25(12). https://www.mdpi.com/1424-8220/25/12/3817.

Pedregosa, F., Varoquaux, G., Gramfort, A., Michel, V., Thirion, B., Grisel, O., Blondel, M., Prettenhofer, P., Weiss, R., Dubourg, V., Vanderplas, J., Passos, A., Cournapeau, D., Brucher, M., Perrot, M., Duchesnay, E., 2011. Scikit-learn: Machine Learning in Python. *Journal of Machine Learning Research*, 12, 2825–2830.

Saadi, S., Simonneaux, V., Boulet, G., Raimbault, B., Mougenot, B., Fanise, P., Ayari, H., Lili-Chabaane, Z., 2015. Monitoring Irrigation Consumption Using High Resolution NDVI Image Time Series: Calibration and Validation in the Kairouan Plain (Tunisia). *Remote Sensing*, 7(10), 13005–13028. https://www.mdpi.com/2072-4292/7/10/13005.

Wang, Y., Xie, D., Zhan, Y., Li, H., Yan, G., Chen, Y., 2021. Assessing the Accuracy of Landsat-MODIS NDVI Fusion with Limited Input Data: A Strategy for Base Data Selection. *Remote Sensing*, 13(2). https://www.mdpi.com/2072-4292/13/2/266.

Xie, Y., Gibbs, H. K., Lark, T. J., 2021. Landsat-based Irrigation Dataset (LANID): 30 m resolution maps of irrigation distribution, frequency, and change for the US, 1997–2017. *Earth System Science Data*, 13(12), 5689–5710. https://essd.copernicus.org/articles/13/5689/2021/.

Zea, P., Pascual, C., García-Montero, L. G., Cedillo, H., 2025. NDVI Performance for Monitoring Agricultural Energy Inputs Using Landsat Imagery: A Study in the Ecuadorian Andes (2012–2023). *Sustainability*, 17(8). https://www.mdpi.com/2071-1050/17/8/3480.